Diagonal tensile tests on historical brick masonry walls strengthened with fabric reinforced cementitious mortar (FRCM)

Pelin E. Mezrea[1], Medine Ispir[2*], Irem A. Balci[3], Ihsan E. Bal[4], and Alper Ilki[5]

[1]Ph.D. Candidate, Department of Civil Engineering, Istanbul Technical University, Istanbul, Turkey, pelinelifmezrea@gmail.com

[2 *](Corresponding author), Assoc. Prof., Department of Civil Engineering, Istanbul Technical University, Istanbul, Turkey, ispirm@itu.edu.tr

[3]MSc, Iller Bankasi A.S., Istanbul, Turkey, iremy@ilbank.gov.tr

[4]Prof. Dr, Research Centre Built Environment, NoorderRuimte, Hanze University of Applied Sciences in Groningen, The Netherlands, i.e.bal@pl.hanze.nl

[5]Prof. Dr., Department of Civil Engineering, Istanbul Technical University, Turkey, ailki@itu.edu.tr

Abstract

Masonry structures comprise a significant portion of the historical building stock all over the world. Previous studies have clearly pointed out that unreinforced masonry buildings are vulnerable against extreme loading conditions, such as seismic actions. Therefore, strengthening is inevitable in most cases for historical masonry to withstand severe loads.

In this paper, the efficiency of fabric reinforced cementitious matrix (FRCM) is investigated experimentally by using diagonal tension tests. Fourteen wallets (750x750x235 mm) were produced. Solid clay bricks, which were collected from the structural walls of an early-20th century building under restoration, and a low-strength mortar, which represents the historical mortar commonly used in similar historical brick masonry buildings located in Istanbul, Turkey, were used to for constructing the specimens. By testing the specimens under monotonic diagonal tension loads, the effects of different types of plasters on the wall surface, varying types of fibers used in textile reinforcement and anchors used for the connection between FRCM and substrate are investigated. Although the wallet samples have inherent shortcomings in representing overall component response accurately, still the qualitative findings are enlightening in terms of the effectiveness of methods as well as failure types.

Keywords Basalt, carbon, diagonal tension, historical, masonry, shear, FRCM

1 Introduction

Earthquakes often cause significant damage or collapse to masonry structures built with traditional methods. In regions with high seismic hazard, like most parts of Turkey, strengthening interventions are inevitable in order to reduce seismic vulnerability, to protect the heritage structures and to avoid possible life losses. As is known, strengthening procedure aims to improve strength and/or deformability of the structural system. Given the inherent difficulties and disadvantages of the traditional strengthening methods (e.g., shotcrete jacketing and prestressed wires), innovative strengthening techniques, such as the use of technical textiles as presented here, have been

reported to be faster, lighter and more efficient methods of structural strengthening. Recent experimental findings indicated that the performance of masonry walls strengthened with fiber-reinforced polymers (FRP) is enhanced remarkably in terms of shear strength and deformability (e.g., Ehsani et al. 1997; Triantafillou 1998; Valluzzi et al. 2002; Faella et al. 2004; Ilki et al. 2008; Tomaževič et al. 2009; Roca and Araiza 2010; Ozsayin et al. 2011; Proença et al. 2012 and Simonič et al. 2015). As a result of extensive and promising research, the demand for technical textiles in industry, together with polymers such as epoxy resins, has increased significantly in recent years. Some negative aspects however prevent using organic binders for historical masonry structures, such as inefficiency at low temperatures and on wet surfaces, lack of vapor permeability, high cost and potential risks to human health. Moreover, the organic binders are incompatible with masonry units in terms of material chemistry and strength, and most importantly, their application is irreversible. ICOMOS Charter- Principles for the Analysis, Conservation and Structural Restoration of Architectural Heritage (2003) emphasizes the concept of the reversibility for the intervention of the historical structures. Application of inorganic binder instead of organic one avoids the aforementioned disadvantages as stated by Kouris and Triantafillou (2018) and Parisi et al. (2019).

Research on seismic upgrade of masonry structures with fabric reinforced cementitious mortar (FRCM) is limited compared to research on strengthening with fiber-reinforced polymers (FRPs). Urban transformation projects, touristic developments of old neighborhoods and re-use projects of historical structures, especially those fro the 19th and the early 20th century in Turkey, led to a large-scale strengthening market for historical masonry structures. Considering the high seismicity in the country, however, the engineering and the scientific practices do not provide many options for effective strengthening of these structures. One of the issues is to find compatible materials. The presented paper thus fills a gap in the literature regarding the experimental evidence on effectiveness of FRCM on a specific composition of historical masonry walls, commonly found in Turkey. There have been previous work on masonry walls strengthened with FRCM, as reported by Prota et al. (2006), Faella et al. (2010), Papanicolaou et al. (2007 and 2011), Parisi et al. (2013), Ismail and Ingham (2014), Babaeidarabad et al. (2014a, b), Sagar et al. (2017), Marcari et al. (2017) and Shabdin et al. (2018). The walls in all these studies were single or double-sided strengthened with carbon, glass or basalt textile grids. The test results were analyzed in terms of the enhancements in shear capacity, ductility and shear modulus and of failure modes. Although the outcome from these studies, applicable to masonry in general, is that FRCM is a promising and efficient alternative strengthening method for masonry walls, these studies do not focus on historical masonry in particular. Historical masonry here refers to the 19th and early 20th century structures built when clay brick and mortar production processes were not regulated, and industrial quality control procedures were not in place. Besides, at the time of construction of these structures, at least in Turkey, seismic regulations and building standards were not in effect. All these practically mean that, although contemporary masonry and historical masonry may seemingly look alike, the mechanical characteristics at material and at structural levels are different. In any case, the number of available studies on FRCM strengthened masonry walls is limited, as reported above, while the characteristics of the masonry structures differ significantly in reality due to the variety of masonry materials and workmanship quality. Hence, in this paper and departing from the rest of the literature, the efficiency of FRCM strengthening method is investigated experimentally for historical brick masonry walls. In this study, original bricks collected from an early 20th century registered historical building for constructing the wall specimens, and a low strength mortar for head/bed joints of the wall specimens, which was designed to represent the mortar commonly used in the similar historical buildings, were used.

Fourteen wallets of dimensions of 750x750x235 mm were constructed. All specimens were tested under monotonic diagonal tension to determine in-plane shear response, qualitative differences among the strengthening methods, and failure modes. Mesh versions of basalt and carbon grids are used to achieve proper adherence with bonding matrix. For bonding textile, mortar is preferred since mortar is economical, compatible with masonry units and recyclable with respect to polymer. Based on the results of the former studies, symmetric (double-sided) strengthening is preferred. The effectiveness and mechanical characteristics of plaster (local and commercial), type of textile (basalt and carbon) and anchorage application are determined experimentally. Although the wallets have inherent limitations in accurately representing the actual behavior at component level, a comparison of an analytical model with ACI 549.4R-13 (2013) is also presented for the sake of completeness.

2 Experimental program

2.1 Specimen description and outline of the tests

The experimental program included fourteen masonry wall specimens. To construct the masonry wall specimens, the traditional masonry construction steps were replicated. As is seen in Fig. 1, each wall was composed of eight brick rows bonded with seven bed mortar joints and five or six head mortar joints in each brick row. The historical clay bricks are 110-120 mm wide, 230-240 mm long and 60-70 mm high. The average dimensions of the brick are indicated in Fig. 2a. The thicknesses of the head and bed joints are 21 and 13 mm, respectively. The nominal dimensions of each wall specimen are thus 750x750x235 mm (Fig. 1). Each masonry specimen has an average thickness of 235 mm equal to the longest dimension of brick for preventing out of plane deformations and adverse slenderness effects (Fig. 1).

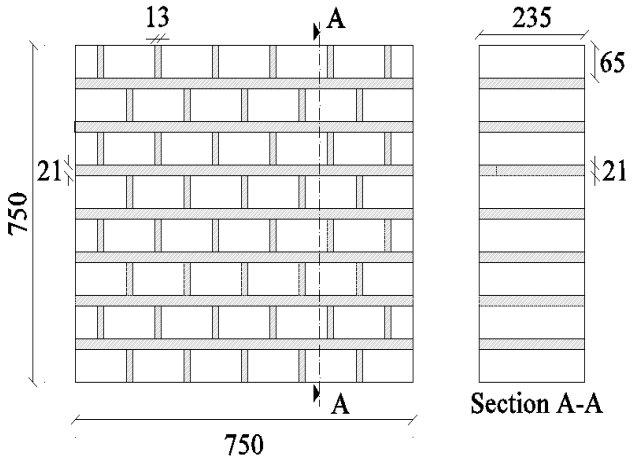

Fig. 1 The configuration of the masonry wall specimen with geometric features (dimensions in mm)

The variables of the test program were chosen as plaster type, fabric type and existence of transverse anchorage, which connected FRCM to the wall surface. The test program and specimen characteristics are presented in Table 1. Local mortar or commercially available cement-based plaster was applied to the surfaces of the walls for plastering. Basalt or carbon grid materials were utilized as strengthening materials and their appearances are shown in Fig. 2c-d. Additionally, to further improve the efficiency of the strengthening intervention, basalt anchorage, which connected FRCM to the wall surface, was applied to several specimens. In

Table 1, the specimens were symbolized in a way to show the test variables. Diagonal test (D)-Fiber type (0 for unconfined state, B for basalt, C for carbon)-Plaster type (0 for without plaster, L for local mortar, T for commercial mortar)-Transverse anchorage (0 for without anchorage, A for showing existence of anchorage)-Number of identical specimens (1 or 2). For example, D-B-T-A (2) shows the second specimen which was strengthened with basalt textile, commercial mortar and anchorage.

Table 1 Experimental program

Specimen code	Specimen series	Plaster type		Strengthening type	
		Local mortar	Commercial mortar	Fiber	Anchorage
D-0-0-0 (1)	Series #1	-	-	-	-
D-0-0-0 (2)		-	-	-	-
D-0-L-0 (1)	Series #2	x	-	-	-
D-0-L-0 (2)		x	-	-	-
D-B-L-0 (1)	Series #3	x	-	Basalt	-
D-B-L-0 (2)		x	-	Basalt	-
D-B-L-A (1)	Series #4	x	-	Basalt	x
D-B-L-A (2)		x	-	Basalt	x
D-B-T-0 (1)	Series #5	-	x	Basalt	-
D-B-T-0 (2)		-	x	Basalt	-
D-B-T-A (1)	Series #6	-	x	Basalt	x
D-B-T-A (2)		-	x	Basalt	x
D-C-T-0 (1)	Series #7	-	x	Carbon	-
D-C-T-0 (2)		-	x	Carbon	-

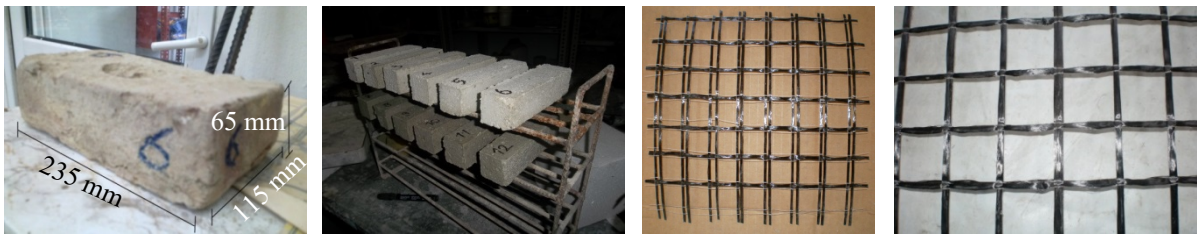

(a) Brick (b) Mortar specimens (c) Basalt open-grid (d) Carbon open-grid

Fig. 2 Samples of the components of the masonry wall

2.2 Material characterization

Flexural bending and compression tests were performed in order to identify the mechanical characteristics of masonry components (brick, joint mortar and plaster mortars). The average flexural tensile strength of six full-size bricks resulted in 1.7 MPa with a coefficient of variation of 0.42 (Mezrea et al. 2016). The average compressive strength of fourteen half bricks was 9.0 MPa with a coefficient of variation of 0.26 (Mezrea et al. 2016). The clay bricks were sampled and tested taking into account ASTM C 67-11 (2011).

Three types of mortar were used in this study for producing head/bead joints and plaster (Table 2). The mortar (Type L* in Table 2) with the mix proportions of 1:2:15:2.9 (cement: lime: sand: water) by weight was used for constructing the bed and head joints. These mix proportions have been adopted from the study of Ispir and Ilki (2013) to properly represent the mortars of historical URM buildings constructed in the 19th and the early 20th

century in Turkey. The low strength is the apparent characteristic of this type historical mortar. With the exception of the water content, these mix-proportions were also adopted to produce local mortar used for plastering of the wall specimens (symbolized with Type L in Table 2) considering the fact that the use of similar materials to the original materials is better for restoration works. The water ratio was increased to 3.72 for ensuring better workability and bonding between the grid fabric and plaster. The second type of plaster (symbolized with T in Table 2) was prepared by using a commercial ready mixed cement-based mortar. This plaster (T) produced with the commercial mortar had the mixing ratios of 2.5:15 (powder: water) by weight. The average flexural and compression strengths of each mortar type were determined experimentally at the ages of 28 and 90 days. For each mortar type, four flexural bending tests and eight compression tests were performed, and their average results are presented in Table 2 (Mezrea et al. 2016). The flexural bending tests were conducted on the specimens with the dimensions of 160x40x40 mm. The compression tests were performed on the specimens, which were the remaining half parts of the flexural test specimens. These tests were realized by considering the prescriptions of TS EN 1015-11 (2000) and ASTM C 348-02 (2002). The main properties of the bidirectional basalt and carbon textile-reinforced mortar are presented in Table 3, which are provided by the supplier based on the report of Trinatafillou (2012). In Tables 2 and 3, StDev and CoV symbolize standard deviation and coefficient of variation, respectively.

Table 2 Mechanical properties of mortar

Mortar type	Age (days)	Flexural tests			Compression tests		
		Average strength (MPa)	StDev (MPa)	CoV	Average strength (MPa)	StDev (MPa)	CoV
Joint: L*	28	0.46	0.02	0.04	1.40	0.30	0.21
	90	0.56	0.03	0.05	1.56	0.19	0.12
Plaster: L (local mortar)	28	0.34	0.06	0.18	0.87	0.08	0.09
	90	0.41	0.02	0.05	1.09	0.03	0.03
Plaster: T (commercial mortar)	28	2.75	0.02	0.01	9.83	0.03	0.003
	90	4.77	0.05	0.01	10.37	0.04	0.004

Table 3 Mechanical characteristics of textile-reinforced mortar composite

Property	Symbol	Units	Basalt FRCM			Carbon FRCM		
			Average	StDev	CoV	Average	StDev	CoV
Modulus of elasticity (un-cracked)	E^*_f	GPa	940	417	0.44	730	147	0.20
Modulus of elasticity (cracked)	E_f	GPa	83.9	17.7	0.21	93.3	10.8	0.12
Ultimate tensile strength	f_{fu}	MPa	1878	205	0.11	1373	203	0.15
Ultimate tensile strain	ε_{fu}	-	0.021	0.0008	0.04	0.017	0.0006	0.04
Fiber area by unit width (one direction)	A_f	mm^2/mm	0.032	-	-	0.061	-	-

2.3 Application of the FRCM system

About six months after the production of the wallets, ten of them were strengthened with different FRCM combinations. By adopting the prescriptions of the supplier, a strengthening procedure with two steps was applied. The first step was to prepare the surfaces of each wall specimen before the application of FRCM system (Fig. 3) and the second was to install the FRCM system (Fig. 4) as detailed in the following paragraphs.

(a) (b) (c)

Fig. 3 Surface preparation (a) grinding, (b) cleaning and (c) soaking

Firstly, the surfaces of each specimen were smoothened by a grinding machine (Fig. 3a), cleaned from remaining particles (Fig. 3b), and soaked with water (Fig. 3c). Secondly, the surfaces of the specimen were plastered with bonding matrix (i.e., local mortar or commercial mortar), Fig. 4a. Then, one layer of the open-grid textile (basalt or carbon) was placed into the plaster on each surface by hand (Fig. 4b), and lastly the textile was covered with a layer of plaster again (Fig. 4c). The composite thickness of the FRCM system was ~18 mm on each surface. Thirty minutes after the completion of this strengthening procedure, the surfaces of the specimen were soaked with water several times to avoid possible shrinkage cracks on mortar.

(a) (b) (c)

Fig. 4 Installation phases of FRCM system (a) plastering, (b) application of open-grid textile, and (c) application of second layer plastering

To investigate the effect of transverse anchor connecting FRCMs onto the surface of the specimen, four specimens (Table 1) were further strengthened with basalt anchors supplied by the manufacturer (Fig. 5a). The locations of the transverse anchors were adjusted according to the known assumption: compression and tension struts of a wall, which are perpendicular to each other, lie along the diagonals of the wall. The details of the basalt anchors are illustrated in Fig. 5b. Firstly, the anchor holes with a diameter of 18 mm and a depth of 75 mm were opened (Fig. 6a). Secondly, these holes were cleaned with air pressure. Thirdly, after each hole was filled with local or commercial mortar, a basalt anchor was pushed with a steel bar into the hole (Fig. 6b-c). Then, to avoid stress concentration around the anchor-end on the surface, the anchor-end was covered with a 200x200mm square patch (Fig. 6d). Finally, the surface of the patch was covered with the finishing layer of plaster.

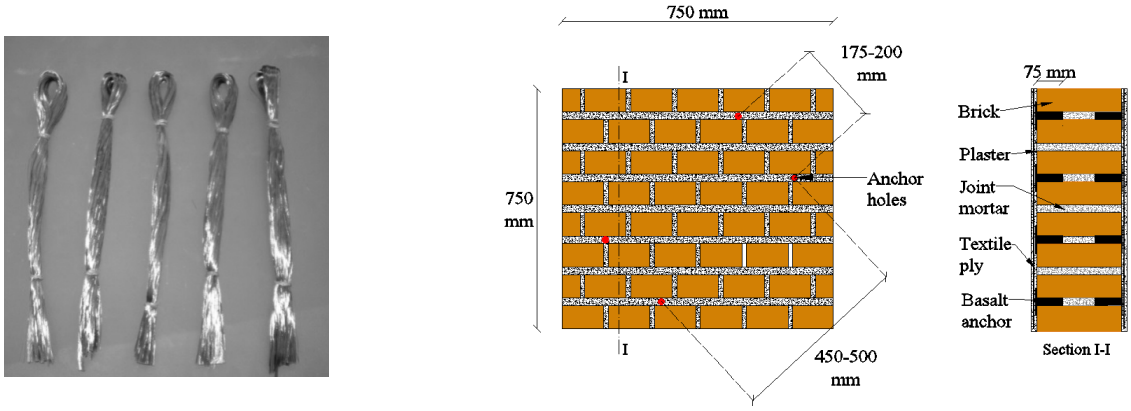

(a) (b)

Fig. 5 Anchorage details (a) basalt anchors, and (b) location of anchor holes

(a) (b) (c) (d)

Fig. 6 Anchorage application (a) anchor holes, (b) installation of anchor, (c) basalt anchor, and (d) square patch

2.4 The test setup

The masonry wall specimens were tested under diagonal compression loading by following ASTM E519/E519M (ASTM International 2010). In order to get the response of each wall, the instrumentation and test setup in Fig. 7a-b were used. The specimen was placed into the test frame by rotating 45˚ (Fig. 7b). A hydraulic jack with a load capacity of 500 kN was used to load the specimen. The applied load was measured by means of a 1000 kN load cell. Linear variable differential transducers (LVDTs) with a 50 mm capacity were installed to record vertical and horizontal deformations (Fig. 7a). Additionally, four LVDTs with a 1000 mm gauge length were also mounted at four corners of the test setup to measure the vertical deformations occurring along the diagonals parallel to the direction of the applied load.

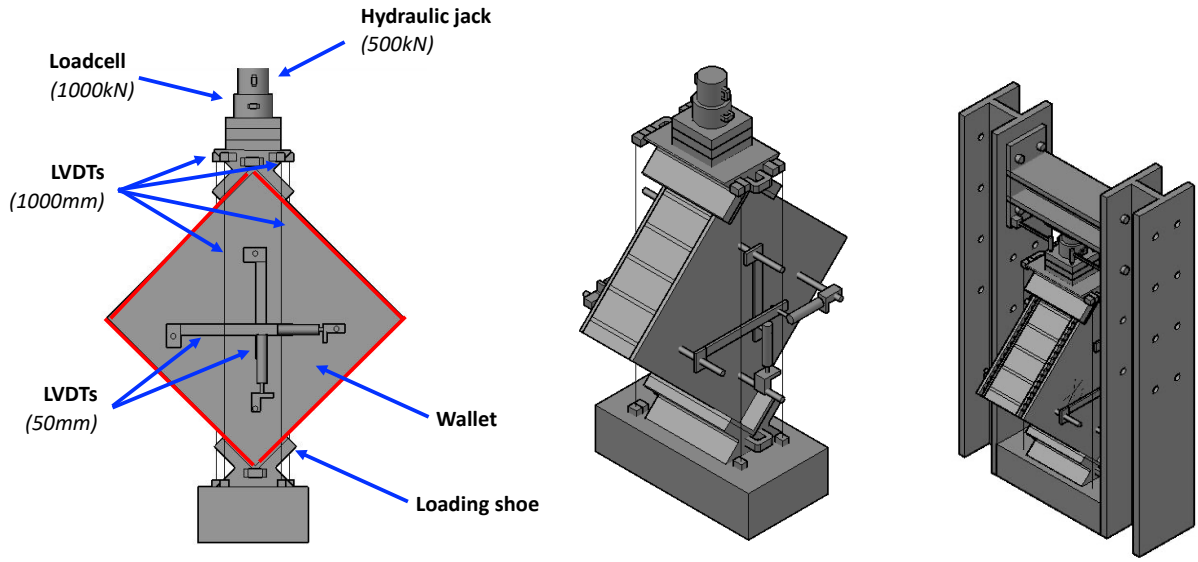

Fig. 7 Diagonal tension test setup and the instrumentation

3 Test results

3.1 Shear stress-shear strain curves

Using the test data obtained from four LVDTs placed in the middle of surfaces of each wall, shear stress-shear strain curve is plotted in Fig. 8a. In order to understand the curve part containing shear strain less than 0.0015, Fig. 8b is also drawn. Shear stress values are calculated using Eq. (1). τ denotes shear stress, P denotes applied load, A_n is the net area of the cross section of the masonry wall, which is computed in accordance with ASTM E519/E519M-10 (2010) using Eq. (2). H and L are the height and length of the specimen, t is the thickness of the specimen and n is the percent of the gross area of the unit. n is computed as 0.97 using the experimental data given in Mezrea (2014) for the solid brick units used in the presented study. Eq. (3) is utilized to compute shear strain values. In Eq. (3), γ denotes shear strain, ΔV denotes vertical displacement, ΔH denotes horizontal displacement and g denotes gauge length.

$$\tau = \frac{P \times cos45°}{A_n} \tag{1}$$

$$A_n = \left(\frac{H+L}{2}\right) tn \tag{2}$$

$$\gamma = \frac{\Delta V + \Delta H}{g} \tag{3}$$

As shown in Fig. 8, the shear stress-shear strain curves of the unstrengthen (i.e. control) and strengthened wallets are trilinear, while the response of the plastered wallets is nearly bilinear, as ideally exhibited in Fig. 9. For the FRCM-strengthened wallets, as the masonry substrate and the FRCM system keep the full integrity between them, the force response keeps increasing, leading to higher strength values eventually. The peak is achieved just before the integrity is lost, and a descending second branch starts ending with a significant strength drop. The last branch is almost a horizontal line up to the total failure of the wallet.

When the second (i.e. descending) branch of the stress-strain curves of the strengthened wallets is examined, it was observed that the significant loss of strength is due to the cracks on the plaster, which in turn reduce the effectiveness of the bond between wall and the FRCM system. Slip type of failure then initiates through a bed mortar joint.

In the FRCM-strengthened specimens, the strength loss ratio for the specimens with local plaster is lower than the ratio for the specimens with commercial plaster. The residual strength is however still significantly higher than the strength of the reference specimens even after the stress drop. This can be attributed to the contribution of the FRCM system even in the final branch.

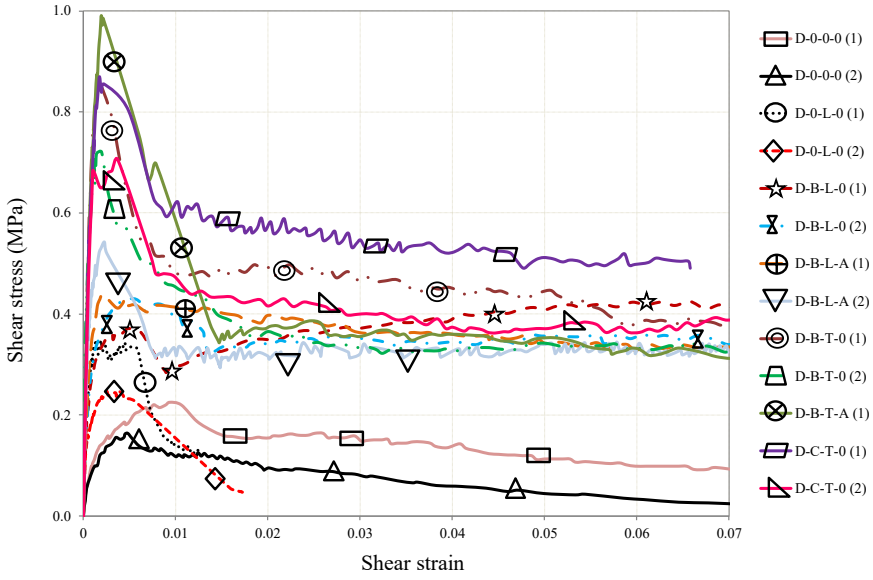

(a)

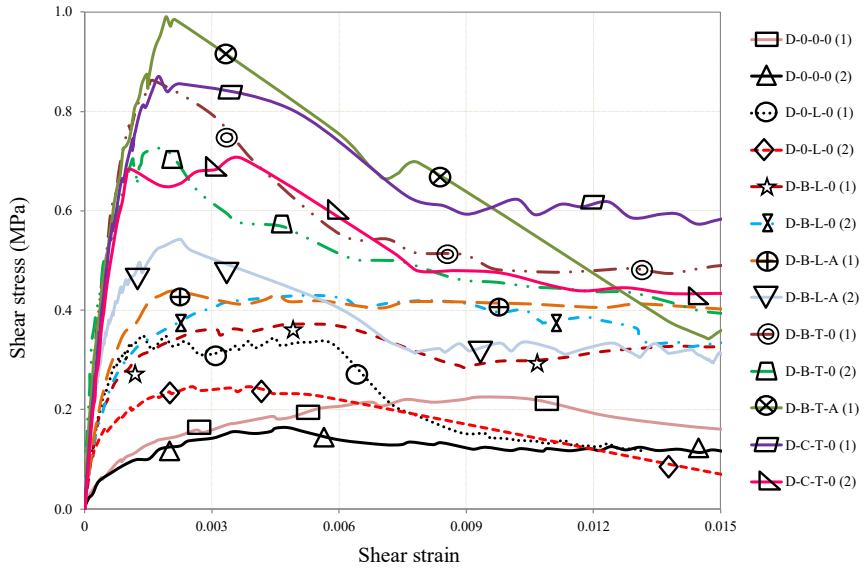

(b)

Fig. 8 Shear stress-shear strain curves

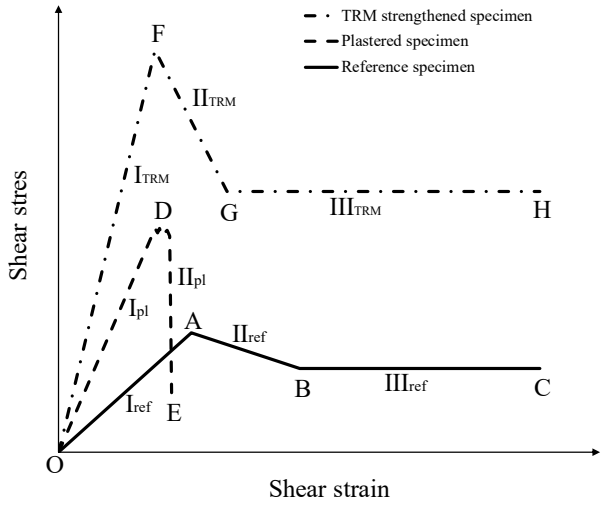

Fig. 9 Idealization of shear stress-shear strain diagrams

The experimentally obtained mechanical characteristics of each masonry wall and corresponding average values of the two identical specimens (denoted as "*av"*) are listed in Tables 4 to 6. Experimental test results are given in terms of unreinforced shear strength (τ_{mo}), shear strength of strengthened specimen (τ_{ms}), shear strain at peak shear stress (γ_{mo} for unreinforced specimen with or without plaster and γ_{ms} for strengthened specimen), shear stress and related strain at the first cracking (τ_{cr} and γ_{cr}), shear modulus (G) and energy dissipation (A). In the literature, the shear stress at the cracking is considered as 75% of the shear strength (Papanicolaou et al. 2007; Babaeidarabad et al. 2014a and Sagar et al. 2017) or 70% of the shear strength (Parisi et al. 2013 and Shabdin et al. 2018). In this study, the shear stress at the cracking was taken as 70% of the shear strength (Table 4). To better represent the ductility of a masonry wall, energy dissipation is used since it is more representative as compared to the ductility ratio that is defined as the ratio of the strains at the specified stress levels. Energy dissipation is calculated as the area under the stress-strain curve enclosed by a specified strain and corresponding stress. In this study, energy dissipation was calculated at different levels of axial strain (0.5, 1.0, 1.5 and 2%) and comparisons are made using the dissipated energy calculated for the area enclosed by 1.5% axial strain (Table 5).

The results presented in this study are based on the average values of the two identical specimens. Highly scattered characteristics of masonry units and/or variety of labor could cause the large variations of strength and strain responses even between the identical masonry wallets (Tables 4-5). For unreinforced masonry wallets, the contribution of plaster to structural behavior can be evaluated by comparison between Series #1-2. Test results show that the local mortar provides 50% enhancement for shear strength and 20% for the dissipated energy with respect to the reference specimens. For the strengthened masonry walls plastered with local mortar, the contribution of FRCM can be evaluated by considering the results of Series #2-3. The enhancements of shear strength and dissipated energy are calculated as 43 and 76%, respectively, with respect to the specimen plastered with local mortar. The influence of the plaster type can be identified with comparing Series #3 with Series #5. The shear strength and dissipated energy of the strengthened specimens with commercial plaster (Series #5) is about 1.8 and 1.6 times higher than that with local plaster (Series #3), respectively. The contribution of the anchor can be determined by taking into account the results of Series #3-Series #4 and Series #5-Series #6. The application of the basalt anchor to the strengthened specimens with local plaster (commercial plaster) provided an additional 14 (39) % in shear strength and 16 (21) % in dissipated energy. Accordingly, the application of the anchor to the

specimens with the plaster having relatively higher strength (commercial plaster) provided more shear strength enhancement. The ratio of the shear strain at peak to the shear strain at cracking may be treated as an indicator of the ductility (Table 4). This ratio is called the pseudo-ductility in Shabdin et al. (2018). According to the average values of these ratios, it is possible to derive that the pseudo-ductility of the specimens with local plaster is higher than that of the specimens with commercial plaster and the specimens with anchorage had lower pseudo-ductility ratios with respect to the specimens without anchorage. Evaluating the results of Series #5 and Series #7 together gives an insight related to the fiber type (basalt and carbon) influence. The fiber type cannot lead to significant differences in the test outcomes (in terms of shear strength and energy dissipation) since the plaster was the weak component of FRCM, cracks were developing in plaster. This prevented basalt and carbon fibers from reaching their ultimate capacities. Among the tested specimens, Series #6 (the specimens strengthened with basalt open grid embedded in commercial plaster and basalt anchor) displayed the best performance in terms of shear strength and dissipated energy. As a conclusion, the evaluation of the tests results leads to the fact that the FRCM system provides significant increase in shear strength, stiffness (shear modulus) and dissipated energy of the historical masonry walls.

Table 4 Shear stress and shear strains of the specimens

Specimen	Specimen code	Series number	τ_{mo} or τ_{ms} (MPa)	γ_{mo} or γ_{ms}	τ_{cr}	γ_{cr}	τ_{ms} / τ_{mo}	γ_{ms} / γ_{cr}
Reference	D-0-0-0 (1)	Series #1	0.23	0.0094	0.16	0.0026	1.15	3.6
	D-0-0-0 (2)		0.16	0.0048	0.11	0.0017	0.80	2.8
	$D\text{-}0\text{-}0\text{-}0_{(av)}$		*0.20*	*0.0071*	*0.14*	*0.0022*	*1.00*	*3.2*
Plaster: Local	D-0-L-0 (1)	Series #2	0.35	0.0019	0.24	0.0005	1.75	3.8
FRCM: -	D-0-L-0 (2)		0.25	0.0025	0.17	0.0006	1.25	4.2
Anchor: -	$D\text{-}0\text{-}L\text{-}0_{(av)}$		*0.30*	*0.0022*	*0.21*	*0.0006*	*1.50*	*3.7*
Plaster: Local	D-B-L-0 (1)	Series #3	0.43	0.0049	0.30	0.0012	2.15	4.1
FRCM: Basalt	D-B-L-0 (2)		0.43	0.0052	0.30	0.0009	2.15	5.8
Anchor: -	$D\text{-}B\text{-}L\text{-}0_{(av)}$		*0.43*	*0.0051*	*0.30*	*0.0011*	*2.15*	*4.6*
Plaster: Local	D-B-L-A (1)	Series #4	0.44	0.0021	0.31	0.0007	2.20	3.0
FRCM: Basalt	D-B-L-A (2)		0.54	0.0023	0.38	0.0006	2.70	3.8
Anchor: Basalt	$D\text{-}B\text{-}L\text{-}A_{(av)}$		*0.49*	*0.0022*	*0.35*	*0.0007*	*2.45*	*3.1*
Plaster: Commercial	D-B-T-0 (1)	Series #5	0.86	0.0016	0.60	0.0006	4.30	2.7
FRCM : Basalt	D-B-T-0 (2)		0.72	0.0020	0.50	0.0005	3.60	4.0
Anchor: -	$D\text{-}B\text{-}T\text{-}0_{(av)}$		*0.79*	*0.0018*	*0.55*	*0.0006*	*3.95*	*3.0*
Plaster: Commercial	D-B-T-A (1)	Series #6	0.99	0.0019	0.69	0.0009	4.95	2.1
FRCM: Basalt	D-B-T-A (2)*		1.20	-	0.84	-	6.00	-
Anchor: Basalt	$D\text{-}B\text{-}T\text{-}A_{(av)}$		*1.10*	-	*0.77*	-	*5.50*	-
Plaster: Commercial	D-C-T-0 (1)	Series #7	0.87	0.0017	0.61	0.0008	4.35	2.1
FRCM: Carbon	D-C-T-0 (2)		0.71	0.0037	0.49	0.0006	3.55	6.2
Anchor:-	$D\text{-}C\text{-}T\text{-}0_{(av)}$		*0.79*	*0.0027*	*0.55*	*0.0007*	*3.95*	3.9

*: Due to experimental error, the test results of D-B-T-A(2) wall with the exception of its shear strength could not be obtained.

Table 5 Dissipated energy capacities of the specimens

Specimen	Specimen code	Series	A ($x10^{-2}$ MPa)

		number	0.5%	1%	1.5%	2%
	D-0-0-0 (1)		0.07	0.20	0.28	0.36
Reference	D-0-0-0 (2)	Series #1	0.06	0.13	0.19	0.24
	$D\text{-}0\text{-}0\text{-}0_{(av)}$		-	-	*0.24*	-
Plaster: Local	D-0-L-0 (1)		0.15	0.27	0.31	-
FRCM: -	D-0-L-0 (2)	Series #2	0.12	-	0.27	-
Anchor: -	$D\text{-}0\text{-}L\text{-}0_{(av)}$		-	-	*0.29*	
Plaster: Local	D-B-L-0 (1)		0.15	0.34	0.47	0.66
FRCM: Basalt	D-B-L-0 (2)	Series #3	0.18	0.40	0.55	0.73
Anchor: -	$D\text{-}B\text{-}L\text{-}0_{(av)}$		-	-	*0.51*	
Plaster: Local	D-B-L-A (1)		0.18	0.42	0.61	0.80
FRCM: Basalt	D-B-L-A (2)	Series #4	0.26	0.41	0.57	0.72
Anchor: Basalt	$D\text{-}B\text{-}L\text{-}A_{(av)}$		-	-	*0.59*	-
Plaster: Commercial	D-B-T-0 (1)		0.29	0.64	0.87	1.11
FRCM : Basalt	D-B-T-0 (2)	Series #5	0.33	0.56	0.74	0.94
Anchor: -	$D\text{-}B\text{-}T\text{-}0_{(av)}$		-	-	*0.81*	-
Plaster: Commercial	D-B-T-A (1)		0.48	0.61	0.98	1.17
FRCM: Basalt	D-B-T-A (2)*	Series #6	-	-	-	-
Anchor: Basalt	$D\text{-}B\text{-}T\text{-}A_{(av)}$		-	-	*0.98*	-
Plaster: Commercial	D-C-T-0 (1)		0.37	0.72	1.00	1.31
FRCM: Carbon	D-C-T-0 (2)	Series #7	0.44	0.56	0.79	1.05
Anchor:-	$D\text{-}C\text{-}T\text{-}0_{(av)}$		-	-	*0.90*	-

Since the modulus is one of the elastic properties of the material, and the shear modulus or modulus of rigidity (G) indicates the stiffness degree of a material, it is computed on the linear part of shear stress-shear strain curve. ASTM E519/519M-10 (2010) defines the modulus as the ratio of shear stress to shear strain, but it does not provide any specified stress-strain range. Hence, some various moduli, which can be considered as chord moduli, were calculated as the slope of the best-fitted line located between the specified shear stress-shear strain points (5-75%, 5-60%, 5-40% and 30-60% of maximum shear stress and corresponding shear strain) and accordingly, the average shear modulus of each series is presented in Table 6. The ratio of the shear stress to shear strain at the cracking, which is accepted as the end of the linear elastic behavior, is also given in Table 6. This can be considered as the secant moduli. As is seen in Table 6, the application of the plaster and/or FRCM system supplied substantial enhancements in the stiffness. Babaeidarabad et al. (2014a) reported that the stiffness increases with the increase in the amount of fabric-reinforced cementitious matrix. The stiffness gains of the FRCM strengthened specimens with commercial plaster is higher than those of the FRCM strengthened specimens with local plaster. The anchorage increased the stiffness of the FRCM strengthened specimens with local plaster. Based on the comparison of the moduli calculated at the different range with the secant moduli at the cracking, it is possible to use the secant modulus at the cracking as shear modulus or the modulus calculated between 5-60% of maximum shear stress on the stress-strain. In the range 5-60% of the maximum shear stress, the average of the modulus of elasticity of URM walls (E) was determined as 184 MPa by Mezrea (2016). By substituting experimental shear and elasticity moduli into Eq. (4), Poisson's ratio (υ) is obtained as 0.20 which can be considered as reasonable. Dizhur and Ingham (2013) calculated the shear modulus of masonry walls as the slope of the line between the 5-70% of the shear

strength on the shear stress-shear strain. Marcari et al. (2017) calculated the shear modulus as the secant modulus between the 5-10% of the strength. Bosiljkov et al. (2005), Borri et al. (2011) and Ismail and Ingham (2014) also experimentally observed considerable variation for the shear modulus. Bosiljkov et al. (2005) also reported that diagonal shear tests are not suitable to assess stiffness features of reinforced masonry, which could explain the significant variation.

Table 6 The shear moduli of the specimens

Specimen series	*G* (MPa)				
	τ_{cr}/γ_{cr}	5-75%	5-60%	5-40%	30-60%
Series #1 (D-0-0-0)	64	50	77	109	55
Series #2 (D-0-L-0)	350	320	424	522	339
Series #3 (D-B-L-0)	273	214	328	531	247
Series #4 (D-B-L-A)	500	474	585	735	483
Series #5 (D-B-T-0)	917	797	1032	1495	755
Series #6 (D-B-T-A)	767	681	830	1082	667
Series #7 (D-C-T-0)	786	788	866	954	785

$$G = \frac{E}{2(1+\upsilon)} \tag{4}$$

3.2 Failure mechanism

The crack development and failure modes of the wallet specimens are described here. Post-test pictures of the unreinforced masonry walls (Series #1 and Series #2) and the strengthened walls with FRCM (Series #3-7) are given in Fig. 10 and Fig. 11, respectively. The initial visible cracks of the reference specimens (Series #1) took place between a brick and a small part of mortar joint around the upper steel shoe (Fig. 10a) just before reaching peak stress (just before Point A indicated in Fig. 9). The load at the visible first crack was around 95% of the maximum load and the width of this crack was 0.3-0.4 mm. After the specimens reached Point A (namely, during the phase of II_{ref} in Fig. 9), the increase in the strain caused to the development of new cracks in a stair-stepped shape following the head and bed joints, and through a bed mortar joint (Fig. 10a-b), and to the crack widening. This level corresponds to a sudden load drop indicated in Fig. 9 (Point B). The drop ratio is about 30% of the peak load. The failure mode, which was progressing gradually, was characterized with the splitting of the specimen into two parts in the stair-stepped shape and a slipping through a bed joint (Fig. 10b). No damage to the bricks was observed when the specimens were examined after the completion of the tests.

In case of the plastered specimens (Series #2), both the wall and the plaster resisted the applied stress up to the level of the shear capacity of the unreinforced masonry wall. When the stress exceeded this level, the masonry became ineffective. The first visible cracks initiated around the upper/lower corners of steel shoes in vertical direction on the plaster just before Point D (Fig. 9). The load at the visible first crack was around 95% of the maximum load and the crack width was 0.2-0.3 mm. Plaster provided the specimen to achieve higher shear capacity with respect to the reference walls and relatively limited the first crack width. The elongation and expansion of the first vertical cracks caused the removal of some parts of the plaster from the surfaces of the specimens. Due to the extending and widening of the crack occurring along a bed joint, the plaster lost its integrity

and the specimens failed suddenly in a brittle manner by exhibiting sliding failure mechanism. Fig. 10c-d shows the crack pattern and failure mode of the plastered specimen.

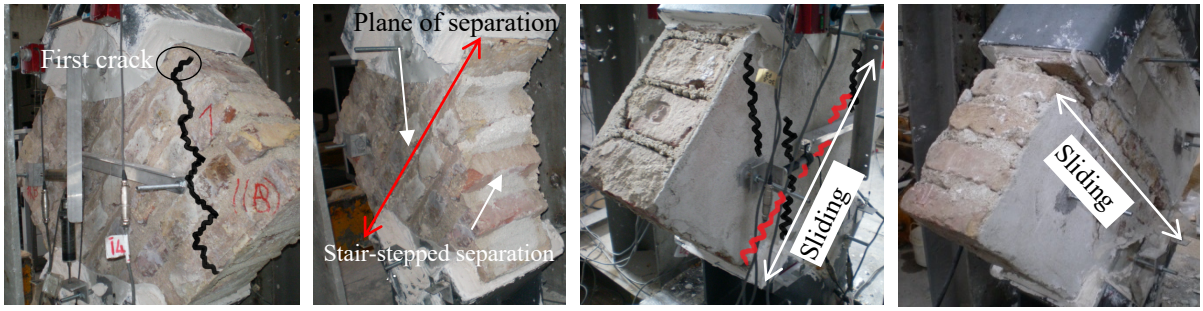

(a) (b) (c) (d)

Fig. 10 Appearances of the reference (a and b) and plastered specimens (c and d) after/during their tests

Fig. 11 exhibits the examples of the post-test shapes of the strengthened specimens. For the strengthened specimens of Series #3, the first visible cracks formed around the upper and lower steel shoes as vertical cracks with a crack width of 0.3-0.4 mm. These cracks took place at 90-95% of the maximum load. The strengthened specimens resisted the applied load up to Point F by maintaining the integrity of masonry wall and FRCM composite (Fig. 9). FRCM strengthening allowed the specimens to withstand high stress values. Just after Point F, FRCM composite (textile grid and plaster) lost its integrity because relatively big parts of plaster fell due to the development of new cracks and widening of existing cracks on the plaster. As strain was increasing, the onset of a stair-stepped separation and/or a shear sliding along a bed joint observed. This level corresponds to a sudden load drop (Point G) indicated in Fig. 9. The drop ratio is about 25% of the peak load. The examination of the specimens after their tests showed the rupture of some grids at the mid-zones of the specimens, the existence of several cracks in bricks near to the lower steel shoe and a local debonding of FRCM around the lower loading plate from the masonry substrate, which was through a height of brick (~70 mm).

The crack development and failure mechanism of Series #4 (D+B+L+A) was almost the same as Series #3. The differences were that the width of the first visible cracks was relatively thin (0.2-0.3 mm), the smaller part of plaster fell, and the local debonding length of FRCM was higher (~180 mm). It is thought that these differences may be due to the use of basalt anchors together with low strength plaster. The crack development of Series #5 (D+B+T) was similar to Series #4. The differences are that the cracks of Series #5 occurred in a smaller region, and the sudden load drop of Series #5 is about 47% of the peak load, which is higher than that of Series #3 and Series #4. This may be due to the use of plaster with relatively high strength. The combination of basalt grid and relatively higher strength plaster (Series #5) provided a higher peak load with respect to Series #3 and Series #4. However, the contribution of FRCM at Point F (Fig. 9) is not sufficient to prevent the load drop or reduce the drop ratio. The crack developments of Series #6 (D+B+T+A) and Series #7 (D+B+C) were similar to Series #5. The differences were that the crack widths of these series were relatively high (0.3-0.4 mm), that no debonding was observed, and that the ratio of the sudden load drop of Series #5 (47%) is lower than that of Series #6 (62%) and higher than that of Series #7 (35%). The fact that the discontinuous anchorage may reduce the connection between FRCM and masonry substrate can result in the higher load drop for Series #6 (D+B+T+A).

In conclusion, the failure mode of the strengthened specimens was governed by shear sliding along a bed joint and/or by a stair-shaped separation parallel to the applied load. Specimens plastered with the commercial

mortar (Series #5-7) had micro cracks on masonry wall surface with respect to the local mortar plastered counterparts (Series #3-4). The sudden degradation ratio of strength for specimens plastered with the commercial mortar (Series #5-7) were higher compared to that for specimens plastered with the local mortar (Series #3-4). The stress-strain relationship of the strengthened specimens is approximately linear at the range III_{FRCM}, which indicates the fibers in FRCM were still effective and provided residual load carrying capacity. Although there is a significant decrease in the load bearing capacity, the shear strength of the specimens strengthened with FRCM is still remarkably higher compared to those of the plastered or reference walls. Although local debonding occurred during some tests, it was not at critical levels to influence the overall behavior. Furthermore, as the dimensions of a real wall will be larger than those of the walls tested here, it is considered that stresses with higher magnitudes will propagate over a larger area and that the problem of debonding will not cause an undesirable situation. Briefly, according to the test results obtained, it could be concluded that the mortar is an appropriate option to develop a good bond between historical masonry substrate and textile grids.

(a) Series #3 (b) Series #4 (c) Series #5 (d) Series #6 (e) Series #7

Fig. 11 Appearances of the failure mechanisms of the strengthened masonry walls

4 Analytical work

4.1 ACI 549.4R-13 (2013) Approach

Although certain limitations exist in wallet tests for reaching widely applicable results, a cross-check with ACI 549.4R-13 (2013) is still provided here for the sake of completeness. According to this, the nominal shear capacity of the wall (V_n) is defined as the sum of the contributions provided by masonry substrate (V_m) and FRCM (V_f) as given in Eq. (5). This equation is established by assuming that FRCM is effective only after the masonry wall cracking (Silva et al. 2008; ACI 549.4R-13 2013; Babaeidarabad et al. 2014a, b).

$$V_n = V_m + V_f \tag{5}$$

The masonry contribution (V_m) is calculated taking into account the possible failure modes of the masonry wall (Li et al. 2005; Silva et al. 2008; Babaeidarabad et al. 2014a, b). The failure modes are shear sliding, shear friction, diagonal tension and toe crushing, which are estimated depending on the geometrical and mechanical properties of the units and the mortar joints. V_m is taken as the minimum of the shear capacities determined with respect to these modes. The possible failure modes and the related expressions to calculate in-plane shear capacity are presented in Table 7. Shear sliding failure is characterized with a crack along a single bed joint due to the bond failure between masonry units and a joint mortar. Shear sliding capacity (V_{ss}) is calculated with the expression

provided in Table 7. In this equation, τ_o is the bond strength between mortar joint and masonry unit, μ_o is the coefficient of shear friction, θ is the inclined angle between horizontal and main diagonal of the wall (degrees).

Table 7 Shear capacity expressions depending on failure modes

Failure mode	Expression	Note
Shear sliding	$V_{ss} = \frac{\tau_o}{1 - \mu_o tan\theta} A_n$	$A_n = \left(\frac{H + L}{2}\right) tn$
Shear friction	$V_{sf} = \frac{\tau_{o,m}}{1 - \mu_m tan\theta} A_n$	$\tau_{o,m} = \frac{\tau_o}{1 + 1.5\mu_o \frac{h}{w}}$ $\mu_m = \frac{\mu_0}{1 + 1.5\mu_o \frac{h}{w}}$
Diagonal tension	$V_{dt} = \frac{tan\theta + \sqrt{21.16 + tan^2\theta}}{10.58} f_t' A_n \left(\frac{L}{H}\right)$	$f_t' = 0.67\sqrt{f_m'}$ (Almeida et al. 2015)
Toe crushing	$V_c = \frac{2wf_m'}{3h + 2wtan\theta} A_m$	

Shear friction failure is appeared in the form of a stepped-stair crack caused by the loss of bond between masonry units and bed/head mortar joints. Shear friction capacity (V_{sf}) is calculated with the expression provided in Table 7. In this equation, $\tau_{o,m}$ is the modified bond strength of the mortar joint, μ_m is the modified coefficient of shear friction, h is the height of the masonry unit and w is the length of the unit.

Diagonal tension failure takes place when the principal tension stress is equal to the tensile strength of the wall. The expression is provided in Table 7 for the calculation of diagonal tension shear capacity (V_{dt}). In this expression, f'_t and f'_m are the tensile and compressive strengths of masonry, respectively. L and H are the length of the masonry wall in the direction of the shear force and the height of the wall, respectively. Toe crushing failure occurs when the stress at a corner equals to the masonry compressive strength. Shear capacity controlled by this type of failure (V_c) is expressed in Table 7. In this expression, A_m is the interface loading area between the steel shoe and the wall. As mentioned above, after calculating shear capacities corresponding to the shear failure modes, the minimum shear load is considered as the shear capacity of the wall, Eq. (6).

$$V_m = \min(V_{ss}, V_{sf}, V_{dt}, V_c) \quad (6)$$

The contribution of FRCM (V_f) to the nominal shear strength of the wall strengthened with FRCM (V_n) is calculated in accordance with ACI 549.4R-13 (2013) as given in Eq. (7). For the determination of the design tensile strength (f_{fv}) and the design tensile strain (ε_{fv}), Eqs. (7-9) are provided by ACI 549.4R-13 (2013).

$$V_f = 2n_f A_f L f_{fv} \quad (7)$$

$$f_{fv} = E_f \varepsilon_{fv} \quad (8)$$

$$\varepsilon_{fv} \leq 0.004 \quad (9)$$

In Eq. (7), n_f is the number of mesh layers, A_f is the area of mesh reinforcement by unit width effective in shear, L is the length of the wall in the direction of applied shear force, f_{fv} is the design tensile strength of FRCM

shear reinforcement, E_f is the tensile modulus of elasticity of the cracked FRCM, and ε_{fv} is the design tensile strain of FRCM shear reinforcement.

For the design, ACI 549.4R-13 (2013) limits the shear load increment provided by FRCM with no more than 50% of the capacity of the unreinforced masonry as given in Eq. (10), and limits the sum of the unreinforced masonry and FRCM shear load capacities with the capacity in case of toe crushing (V_c) as is seen in Eq. (11).

$$V_f = \min(2n_f A_f L f_{fv}; 0.5V_m) \quad (10)$$

$$V_n = \min(V_m + V_f; V_c) \quad (11)$$

4.2 Estimation of the shear strength

Following the approach presented above, the shear strength of the specimens are calculated and compared to the experimental results. The geometrical and mechanical characteristics of a masonry wall, which are required for the estimations, are as follows: the height (H), length (L) and thickness (t) of the specimen are 750, 750 and 235 mm, respectively. The dimensions of the brick units (h and w) are taken as the average of the corresponding ranges (65 and 115 mm). The angle between horizontal and main diagonal of the wall (θ) is taken as 45°. Substituting the geometrical characteristics of the wall into Eq. (2), A_n is calculated as 170,963 mm^2. The interface loading area between the steel shoe and the wall (A_m) is calculated as 40,420 mm^2. It should be noted that the net length of the steel shoe is 86 mm. Considering the properties of the masonry wall, τ_o and μ_o are assumed as 0.15 MPa and 0.4, respectively, in accordance with TSDC (Disaster and Emergency Management Authority, 2018). f'_m was determined as 1.6 MPa in Mezrea et al. (2016) for the unreinforced masonry wall constructed with the same brick units and bed/head joint mortars as the presented study. Using the expression given in Table 7, f'_t is calculated as 0.85 MPa.

Using the expressions in Table 7, the shear capacities of the unreinforced masonry wall without plaster are calculated as 42.7, 27.3, 78.2 and 35.0 MPa due to the failures of shear sliding, shear friction, diagonal tension and toe crushing, respectively. In accordance with Eq. (6), the nominal shear capacity of the wall is 27.3 kN due to the shear friction failure. The experimentally obtained shear strength of the wall is 33 kN by exhibiting a combined failure mechanism of the shear friction and shear sliding failure. It is considered that the plaster contribution (V_p) should also be taken into account when calculating the shear capacity of the plastered specimens. For this, the approach presented by Almeida et al. (2015) is adopted (Eq. 12). The approach estimates the plaster contribution using the expression given in Table 7 for diagonal tension failure. Accordingly, V_p and nominal shear capacity of the wall ($V_{m,p}$) with local plastering are computed as 6.0 and 33.3 kN, respectively. The experimental shear capacity of URM wall with local plastering is 53.8 kN due to shear sliding. V_p and $V_{m,p}$ of the wall with commercial plastering are computed as 69.5 and 96.8 kN, respectively. The ratios of experimental shear capacity to analytical one (E/A) are given in Table 8 for the URM wall with and without plastering. The difference between analytical and experimental shear capacities may be due to the combined failure mechanisms observed in the tests.

$$V_{m,p} = V_m + V_p \quad (12)$$

The contribution of FRCM composite material (V_f) to the shear capacity is calculated using Eqs. (6-9). For the specimens strengthened with basalt and carbon FRCM, the values of V_f are calculated as 32.2 and 68.3 kN, respectively. Then, using Eq. (5), the nominal shear capacities of the masonry walls strengthened with FRCM are

calculated and presented in Table 8. It should be noted that while using Eq. (5), the contribution of plaster is considered by substituting $V_{m,p}$ in place of V_m. As is seen in Table 8, the *E/A* ratios for the strengthened specimens are calculated in the range of 0.9-1.2. These ratios indicates that the analytical results are in good agreement with the experimental results. To use the allowable maximum tensile strain (0.004) and to consider plaster contribution in the analytical estimations may be ensured this agreement. Accepting the fiber tensile strain of 0.004 may be realistic because the cracking in the plaster prevented the fibers from reaching their ultimate tensile strain capacities.

The analytical estimations listed in Table 8 is calculated based on the allowable maximum tensile strain (0.004) prescribed by ACI 549.4R-13 (2013). Adopting this allowable strain and no considering plaster contribution, the *E/A* ratios were calculated between 1.3-1.6 by Babaeidarabad et al. (2014a), 2.3 by Almeida et al. (2015) and 1.5 by Sagar et al. (2017). Almeida et al. (2015) calculated the *E/A* ratio as 1.5 by considering the plaster contribution.

When following ACI 549.4R-13 (2013) design limits given in Eqs. (9-10), the nominal shear capacity of all strengthened walls are calculated as 35 kN, and the governing failure mode is determined as toe crushing. In this state, the *E/A* ratios are between 2.2 and 4.2. Adopting these design limits of ACI 549.4R-13 (2013), Babaeidarabad et al. (2014a) calculated *E/A* ratios as 2.9 and 3.5. The ratios calculated here (2.2-4.2) and calculated by Babaeidarabad et al. (2014a) indicate that the design approach of ACI 549.4R-13 (2013) is conservative.

Table 8 The shear capacity of the masonry walls tested

Specimen	Experimental (*E*) *V* (kN)	Analytical (*A*) *V* (kN)	*E/A* Ratio
D-O-O-O	33.3	27.8	1.2
D-O-L-O	53.8	33.8	1.6
D-B-L-O	76.2	65.5	1.2
D-B-T-O	146.6	129.0	1.1
D-C-T-O	144.8	165.1	0.9

5 Conclusions

Effectiveness of fabric reinforced cementitious mortar (FRCM) strengthening method is investigated for the shear behavior of the historical brick masonry walls in this study. The specimens were built with authentic historical solid clay bricks and original-like low-strength mortar. The mortar is considered to represent the historical mortar commonly used in the typical walls of the 19th and early 20th century historical URM buildings built in Turkey. Diagonal tension tests of fourteen specimens were performed with the aim of gaining insights regarding the effect of plaster type, fiber type and presence of anchorage on the shear behavior of the tested walls.

The test results exhibit a significant influence on the mechanical characteristics by the plaster. The use of commercial plaster, which has higher compressive/tensile strength with respect to the local plaster, led to higher shear strength and dissipated energy capacities with respect to the local plaster. The average shear strength and dissipated energy capacities of the FRCM specimens plastered with commercial mortar are 1.84 and 1.59 times higher than those of the specimens plastered with local mortar, respectively.

Although different fibers (i.e. carbon and basalt) have been used in the tests, the difference was not apparent. This is due to the early cracking of the plaster, a characteristic response of FRCM strengthened walls, an issue that hinders the influence of the fiber type. The crack development and failure mechanisms have thus been similar for the specimens strengthened with basalt and carbon fibers. The only difference presented itself in the average ratio of the load drop, where FRCM specimens with basalt fibers had 1.34 times higher drop than that of the specimens with carbon fibers.

The application of the basalt anchor presented an additional improvement in shear strength and dissipated energy, especially in the specimens plastered with commercial mortar having higher compressive/tensile strengths with respect to the local mortar. In case of the FRCM specimens plastered with the local mortar, average shear strength and dissipated energy capacities of the FRCM specimens with anchors were 1.15 and 1.14 times higher than those of the specimens without anchors, respectively. In case of the FRCM specimens plastered with the commercial mortar, average shear strength and dissipated energy capacities of the FRCM specimens with anchors were 1.21 and 1.39 times higher than those of the specimens without anchors, respectively.

The responses of the tested specimens clearly indicate that the strengthening of historical brick masonry walls with FRCM system is an efficient and promising alternative to improve lateral resistance in terms of shear strength and dissipated energy. Future studies should focus on possible measures to prevent the abrupt strength drops and possible ways of increasing the effectiveness of the anchors.

Acknowledgements

The experimental research was carried out at The Structural and Earthquake Engineering Laboratory of Istanbul Technical University. The authors would like to thank ITU Scientific Research Office, Fyfe Europe S.A. and Tekstar Ltd. The contributions of technical staff of the laboratory are acknowledged. Special thanks go to Cem Demir, Ergün Binbir, Korhan Deniz Dalgic and Ali Osman Ates for their helpful assistance and discussions.

References

ACI Committee 549.4R-13 (2013) Guide to design and construction of externally bonded fabric – reinforced cementitious matrix (FRCM) systems for repair and strengthening concrete and masonry structures (ACI 549.4R-13). American Concrete Institute, Farmington Hills, MI

Almeida JA, Pereira EB, Barros JA (2015) Assessment of overlay masonry strengthening system under in-plane monotonic and cyclic loading using the diagonal tensile test. Constr Build Mater 94:851-865

ASTM C 348-02 (2002) Standard test methods for flexural strength of hydraulic cement mortars. American Society for Testing Materials, USA

ASTM C 67-11 (2011) Standard test methods for sampling and testing brick and structural clay tile. American Society for Testing Materials, USA

ASTM E519/E519M-10 (2010) Standard test method for diagonal tension (shear) in masonry assemblages. American Society for Testing Materials, USA

Babaeidarabad S, Arboleda D, Loreto G, Nanni A (2014a) Shear strengthening of un-reinforced concrete masonry walls with fabric-reinforced-cementitious matrix. Constr Build Mater 65:243–253

Babaeidarabad S, De Caso F, Nanni A (2014b) URM walls strengthened with fabric-reinforced cementitious matrix composite subjected to diagonal compression. J Compos Constr ASCE 18(2), 04013045

Borri A, Castori G, Corradi M, Speranzini E (2011) Shear behavior of unreinforced and reinforced masonry masonry walls subjected to in situ diagonal compression tests. Constr Build Mater 25:4403-4414

Bosiljkov VZ, Totoev YZ, Nichols JM (2005) Shear modulus and stiffness of brickwork masonry: an experimental perspective. Struct Eng Mech 20(1):21–43

Dizhur D, Ingham JM. (2013) Diagonal tension strength of vintage unreinforced clay brick masonry wall panels. Constr Build Mater; 43(6):418–27

Ehsani MR, Saadatmanesh H, Al-Saidy A (1997) Shear behavior of URM retrofitted with FRP overlays. J Compos Constr 1(1):17–25

Faella C, Martinelli E, Nigro E, Paciello S (2004) Tuff masonry walls strengthened with a new kind of C-FRP sheet: experimental tests and analysis. In: Proceedings of the 13th World conference on earthquake engineering, paper no 923

Faella C, Martinelli E, Nigro E, Paciello S (2010) Shear capacity of masonry walls externally strengthened by a cement-based composite material: An experimental campaign. Constr Build Mater; 24:84–93

ICOMOS Charter- Principles for the Analysis, Conservation and Structural Restoration of Architectural Heritage (2003). Ratified by the ICOMOS 14th General Assembly in Victoria Falls, Zimbabwe.

Ilki A, Ispir M, As F, Demir C, Kumbasar N (2008) FRP retrofit of walls constructed with historical bricks. In: Proceedings of the Challenges for Civil Construction, Porto, Portogual, April 16-18

Ismail N, Ingham MJ (2014) Polymer textiles as a retrofit material for masonry walls. Structures and Buildings, 167(1):15-25

Ispir M, Ilki A (2013) Behavior of historical unreinforced brick masonry walls under monotonic and cyclic compression. The Arabian Journal for Science and Engineering 38(8):1993-2007

Kouris LAS, Triantafillou TC. (2018) State-of-the-art on strengthening of masonry structures with textile reinforced mortar (FRCM). Constr Build Mater 188:1221-1233

Li T, Galati N, Tumialan JG, Nanni A (2005) Analysis of unreinforced masonry concrete walls strengthened with glass fiber-reinforced polymer bars. ACI Struct J 102(4):569–577

Marcari G, Basili M, Vestroni F (2017) Experimental investigation of tuff masonry panels reinforced with surface bonded basalt textile-reinforced mortar. Compos. B Eng. 108:131–142

Mezrea PE, Yilmaz IA, Ispir M, Bal IE, Ilki A (2016) External jacketing of unreinforced historical masonry piers with open-grid basalt reinforced mortar. ASCE, J Compos Construct. 04016110

Mezrea, PE (2014) Retrofitting of historical brick masonry walls with textile reinforced mortar (FRCM). MSc thesis, submitted to Istanbul Technical University Graduate School of Science Engineering and Technology, (in Turkish)

Disaster and Emergency Management Authority, (2018) Turkish seismic design code (TSDC). Ankara, Turkey, (in Turkish)

Ozsayin B, Yilmaz E, Ispir M, Ozkaynak H, Yuksel E, Ilki A (2011) Characteristics of CFRP retrofitted hollow brick infill walls of reinforced concrete frames. Constr Build Mater, 25(10):4017-4024

Papanicolaou CG, Triantafillou TC, Karlos K, Lekka M (2011) Externally bonded grids as strengthening and seismic retrofitting materials of masonry masonry walls. Construct Build Mater 25:504–514

Papanicolaou CG, Triantafillou TC, Karlos K, Papathanasiou M (2007) Textile-reinforced mortar (FRCM) versus FRP as strengthening material of URM walls: in-plane cyclic loading. Mater and Struct 40:1081–1097

Parisi F, Costantino M, Prota A (2019) Fabric-Reinforced Cementitious Matrix (FRCM) composites: Mechanical behavior and application to masonry walls. Failure Analysis in Biocomposites, Fibre-Reinforced Composites and Hybrid Composites, Woodhead Publishing Series in Composites Science and Engineering 199-227.

Parisi F, Iovinella I, Balsamo A, Augenti N, Prota A (2013) In-plane behaviour of tuff masonry strengthened with inorganic matrix–grid composites. Compos. B Eng. 45 (1):1657–1666

Proença J, Gago AS, Cardoso J, Cóias V, Paula R (2012) Development of an innovative seismic strengthening technique for traditional load-bearing masonry walls. Bull Earthquake Eng 10:113-133

Prota A, Marcari G , Fabbrocina G, Manfredi G, Aldea C (2006) Experimental in-plane behavior of tuff masonry strengthened with cementitious matrix-grid composites. J Compos Constr ASCE 10(3):223-233

Roca P, Araiza G (2010) Shear response of brick masonry small assemblages strengthened with bonded FRP laminates for in-plane reinforcement. Construct Build Mater 24:1372–1384

Sagar SL, Singhal V, Rai DC, Gudur P (2017) Diagonal shear and out-of-plane flexural strength of fabric-reinforced cementitious matrix-strengthened masonry walletes. J Compos Constr 21(4):04017016

Shabdin M, Zargaran M, Attari NKA (2018) Experimental diagonal tension (shear) test of Un-Reinforced Masonry (URM) walls strengthened with textile reinforced mortar (FRCM). Constr Build Mater 164:704–715

Silva PF, Yu P, Nanni A (2008) Monte Carlo simulation for validating the in plane shear capacity of URM walls strengthened with GFRP grid reinforced polyuria. J Composfor Construct 12(4):405–415

Simonič JM, Gostič S, Bosiljkov V, Žarnić R (2015) In-situ and laboratory tests of old brick masonry strengthened with FRP in innovative configurations and design considerations. Bull Earthquake Eng 13:257-278

Tomaževič M, Klemenc I, Weiss P (2009) Seismic upgrading of old masonry buildings by seismic isolation and CFRP laminates: a shaking-table study of reduced scale models. Bull Earthquake Eng 7: 293-321

Triantafillou TC (1998) Strengthening of masonry structures using epoxy-bonded FRP laminates. J Compos Construct ASCE 2(2):96–104

Trinatafillou T. (2012) Tensile Properties of Tyfo® RM (Reinforced Mortar) System. University of Patras, Greece. Technical report prepared for Fyfe Europe

TS EN 1015-11, 2000. Methods of test for mortar for masonry- Part 11: Determination of flexural and compressive strength of hardened (in Turkish). Turkish Standards Institution, Ankara.

Valluzzi MR, Tinazzi D, Modena C (2002) Shear behaviour of masonry walls strengthened by FRP laminates. Constr Build Mater 16(7):409–416